

• Original Paper •

# Investigating the Initial Errors that Cause Predictability Barriers for Indian Ocean Dipole Events Using CMIP5 Model Outputs

Rong FENG<sup>1</sup> and Wansuo DUAN<sup>\*1,2</sup><sup>1</sup>*LASG, Institute of Atmospheric Physics, Chinese Academy of Sciences, Beijing 100029, China*<sup>2</sup>*University of Chinese Academy of Sciences, Beijing 100049, China*

(Received 5 September 2017; revised 18 January 2018; accepted 6 March 2018)

## ABSTRACT

By analyzing the outputs of the pre-industrial control runs of four models within phase 5 of the Coupled Model Inter-comparison Project, the effects of initial sea temperature errors on the predictability of Indian Ocean Dipole events were identified. The initial errors cause a significant winter predictability barrier (WPB) or summer predictability barrier (SPB). The WPB is closely related with the initial errors in the tropical Indian Ocean, where two types of WPB-related initial errors display opposite patterns and a west–east dipole. In contrast, the occurrence of the SPB is mainly caused by initial errors in the tropical Pacific Ocean, where two types of SPB-related initial errors exhibit opposite patterns, with one pole in the subsurface western Pacific Ocean and the other in the upper eastern Pacific Ocean. Both of the WPB-related initial errors grow the fastest in winter, because the coupled system is at its weakest, and finally cause a significant WPB. The SPB-related initial errors develop into a La Niña-like mode in the Pacific Ocean. The negative SST errors in the Pacific Ocean induce westerly wind anomalies in the Indian Ocean by modulating the Walker circulation in the tropical oceans. The westerly wind anomalies first cool the sea surface water in the eastern Indian Ocean. When the climatological wind direction reverses in summer, the wind anomalies in turn warm the sea surface water, finally causing a significant SPB. Therefore, in addition to the spatial patterns of the initial errors, the climatological conditions also play an important role in causing a significant predictability barrier.

**Key words:** predictability barrier, initial errors, Indian Ocean Dipole, targeted observations

**Citation:** Feng, R., and W. S. Duan, 2018: Investigating the initial errors that cause predictability barriers for Indian Ocean Dipole events using CMIP5 model outputs. *Adv. Atmos. Sci.*, **35**(10), 1305–1320, <https://doi.org/10.1007/s00376-018-7214-7>.

## 1. Introduction

It is well known that tropical oceans play an important role in modulating global climate variability. The El Niño–Southern Oscillation (ENSO), as the strongest ocean–atmosphere coupled signal on interannual time scales in the tropical Pacific Ocean, has attracted a lot of attention for decades (Jin, 1997; Weiss and Weiss, 1999; Duan and Mu, 2006; Mu et al., 2007; Duan et al., 2009). In contrast, the Indian Ocean Dipole (IOD) was first identified in the 1990s (Saji et al., 1999; Webster et al., 1999) and is a west–east seesaw pattern of sea surface temperature anomalies (SSTAs) in the tropical Indian Ocean accompanied by wind anomalies at the equator. The IOD usually develops in spring and summer, peaks in autumn, and finally decays rapidly in winter (Saji et al., 1999; Webster et al., 1999; Li et al., 2002, 2003; Krishnamurthy and Kirtman, 2003; Lau and Nath, 2004; Cai et al., 2005; Behera et al., 2006). In the positive phase of IOD

events, there are generally high (low) land surface temperatures and more (less) precipitation over the west (east) coast of the Indian Ocean, and vice versa for negative IOD events (Ashok et al., 2001). Furthermore, IOD events also modulate the climate in distant regions, such as Europe, North-east Asia, North America, South America and South Africa, by the propagation of planetary waves (Birkett et al., 1999; Ansell et al., 2000; Clark et al., 2003; Saji and Yamagata, 2003; Behera et al., 2005). Studying the predictability of IOD events is therefore useful and timely.

Many studies have demonstrated that the lead time for skillful IOD predictions is only one season, which can be prolonged to two seasons for strong events (Luo et al., 2007). The reasons for the low forecast skill of IOD events are still not clear. On the one hand, many models cannot accurately describe the dynamical processes closely related to the IOD, and thus cannot simulate its basic characteristics (Feng et al., 2014a). On the other hand, the IOD in itself may also be more difficult to predict than ENSO and is affected by more complex physical processes. The IOD interacts strongly with the Asian–Australian monsoon (Yoo et al., 2006; Yang et al.,

\* Corresponding author: Wansuo DUAN  
Email: duanws@lasg.iap.ac.cn

2010; Jourdain et al., 2013). Furthermore, there are chaotic intraseasonal oscillations in both the ocean and the atmosphere (Masumoto et al., 2005; Han et al., 2006). These random forcings and highly nonlinear characteristics make IOD forecasts a challenge.

Beyond that, the existence of the winter predictability barrier (WPB) also greatly limits the forecast skill of IOD events (Luo et al., 2007; Feng et al., 2014b). From a statistical perspective, the WPB means that whatever the start month, the forecast skill decreases quickly across winter (Luo et al., 2007). In terms of error growth, the WPB is a phenomenon where the prediction errors grow fastest in winter and cause large prediction uncertainties (Feng et al., 2014b). Using the Geophysical Fluid Dynamics Laboratory Climate Model version 2p1 (GFDL-CM2p1), Feng et al. (2017) found that initial temperature errors with a west–east dipole pattern at the sea surface and at 95 m depth in the tropical Indian Ocean are more inclined to cause a significant WPB than other initial errors. The largest values of the dipole pattern initial errors are concentrated in a small area (i.e., the subsurface eastern tropical Indian ocean), which is likely the sensitive area for targeted observations of IOD events. That is, if intensive observations are carried out over this area and assimilated into the initial field, the prediction errors of IOD events will most likely be reduced and the forecast skill improved. Similar conclusions were also obtained by Feng and Duan (2017) based on observations.

The Indian Ocean is closely connected with the Pacific Ocean by an atmospheric bridge (i.e., the Walker circulation; Chen, 2010; Lian et al., 2014) and by the Indonesian through-flow (Lee et al., 2002). Previous studies have found that about two thirds of IOD occurrences are accompanied by ENSO (Loschnigg et al., 2003; Stuecker et al., 2017). The strength of the IOD relies strongly on the strength of ENSO in model simulations (Liu et al., 2014). Therefore, the Pacific Ocean probably plays an important role in IOD predictions. Omitting the full consideration of the role of the Pacific Ocean in IOD predictions may be another reason for the low forecast skill of IOD events.

Considering that previous studies only explored the effects of initial errors on the predictability of IOD events in the tropical Indian Ocean, and that the Pacific Ocean probably plays an important role in IOD predictions, the combined effects of initial errors in both oceans on IOD predictions should be studied. As positive IOD events are usually stronger and have larger climatic effects than negative ones, only positive IOD events are analyzed in this study (Vinayachandran et al., 2002; Ashok et al., 2003; Guan and Yamagata, 2003; Annamalai and Murtugudde, 2004; Behera et al., 2005; Cai et al., 2009). We aimed to answer the following questions regarding positive IOD events:

(1) Does the predictability barrier exist in predictions of positive IOD events when considering the initial errors in the tropical Indian and Pacific oceans? If so, what are the spatial patterns of the initial errors related to the predictability barrier? Are they the same as when only considering the initial errors in the tropical Indian Ocean?

(2) What useful information can these initial errors provide for improving the forecast skill of positive IOD events?

We studied these questions using the outputs of several models within phase 5 of the Coupled Model Intercomparison Project (CMIP5; more details available at <http://cmip-pcmdi.llnl.gov/cmip5>). The remainder of the paper is organized as follows: The strategy and model descriptions are provided in section 2. The spatial patterns of the predictability barrier-related initial errors and their physical mechanisms for development are explored in section 3. The implications of these initial errors for IOD predictions in the context of targeted observations are discussed in section 4. Finally, a summary and discussion are provided in section 5.

## 2. Strategy

We used the outputs of the pre-industrial (PI) control runs within CMIP5 to explore the effects of the initial errors on the predictability of positive IOD events. PI control runs indicate that all forcings of the runs are time-invariant and fixed at 1850 levels (Taylor et al., 2012). Fourteen CMIP5 models that have often been used to project the properties of IOD events (Cai and Cowan, 2013; Weller and Cai, 2013a, 2013b; Zheng et al., 2013) were selected and evaluated (figures omitted). It was found that most models simulate an excessively large IOD amplitude with an overly strong thermocline–SST feedback compared with observations, which is consistent with previous studies (Cai and Cowan, 2013; Liu et al., 2014; Li et al., 2015). Among the 14 CMIP5 models, only five models, which capture the climatological conditions well in the tropical Indian Ocean, could reproduce the winter persistence barrier phenomenon of positive IOD events in both the growing and decaying phases (Feng et al., 2014a). These models are GFDL-CM2p1, CanESM2, MPI-ESM-LR, MIROC5, and CSIRO Mk3.6.0. As there are no PI control runs for GFDL-CM2p1, only the other four models were selected. Furthermore, all these four models simulate the interaction between the IOD and ENSO well (figures omitted), and thus were applied in this study to discuss the effect of initial errors in these two basins on IOD predictability. The monthly mean data of sea temperature and sea surface winds (at 10 m height) were derived in these four models. Details of the models are listed in Table 1.

The experimental strategy was the same as employed in Feng and Duan (2017). Therefore, we describe it only briefly here. Positive IOD events were randomly chosen from the 200-year outputs in each model according to the definition by Saji and Yamagata (2003). For each positive IOD, the sea temperatures were assumed to be an “observation” to be predicted, and the sea temperatures in the 20 years around the “observed” year were taken as “predictions” of this “observation”. That is, there were 20 “predictions” for each “observation” with different initial fields. The predictions started from July(–1), October(–1), and January(0), with a lead time of 12 months [where (–1) indicates the year preceding the reference IOD year, and (0) indicates the reference IOD year].

**Table 1.** Brief description of the four models from CMIP5 used in this study.

Model	Institute	Resolution		Data length
		Atmosphere	Ocean <sup>a</sup>	
CSIRO Mk3.6.0	CSIRO Marine and Atmospheric Research in collaboration with the Queensland Climate Change Centre of Excellence (QCCCE)	T63	0.9375° × 1.875°	200 yr
CanESM2	Canadian Centre for Climate Modeling and Analysis (CCCma)	T63	0.9375° × 1.41°	200 yr
MIROC5	Atmosphere and Ocean Research Institute (AORI), University of Tokyo; National Institute for Environmental Studies (NIES); Japan Agency for Marine-Earth Science and Technology (JAMSTEC)	T85	0.5° × 1.4°	200 yr
MPI-ESM-LR	Max Planck Institute for Meteorology	T63	1.5° × 1.5°	200 yr

<sup>a</sup>Degrees latitude × longitude; only the ocean resolution at the latitude closest to the Equator is shown.

As the results for different start months were the same, the start month of October(−1) is taken as an example in the following discussion. For the start month of October(−1), the sea temperatures from October(−1) to September(0) in each reference IOD year are defined as an “observation”, and the sea temperatures from October(−2) to September(−1) [where (−2) indicates the year preceding year (−1)] are assumed to be one of the 20 predictions, and so on (Fig. 1). The absolute values of the difference between the “predicted” and the “observed” Dipole Mode Indexes (Saji et al., 1999) are defined as the prediction errors. As there are no model errors, the prediction errors are caused only by the initial errors. The growth rates of prediction errors  $\eta$  are defined as

$$\eta = \frac{\partial E(t)}{\partial t} \approx \frac{E(t_2) - E(t_1)}{t_2 - t_1}, \quad (1)$$

where  $E(t_1)$  and  $E(t_2)$  are the prediction errors at times  $t_1$  and  $t_2$ . The difference between  $t_2$  and  $t_1$  is one month, which is sufficiently small. When the value of  $\eta$  is positive, the prediction errors increase, and vice versa for negative  $\eta$ . As the prediction errors are only caused by initial errors, the first type

of predictability issues is analyzed to study the effects of initial errors on IOD predictability. The initial errors are defined as the difference between the “predicted” and the “observed” sea temperatures in the tropical Indian and Pacific oceans in October(−1).

### 3. Results

We analyzed the season-dependent evolution of the prediction errors for positive IOD events and identified the initial errors that cause significant predictability barriers in IOD predictions. Moreover, by tracing the evolution of sea temperature and wind anomalies, we discuss the physical mechanisms of development for these predictability barrier-related initial errors.

#### 3.1. Season-dependent evolution of prediction errors caused by initial errors

Based on the method in section 2, the prediction errors for each positive IOD event in the four models were calculated. Figure 2 shows the ensemble mean of the error growth rates for each positive IOD event in the four models. The error growth rates,  $\eta$ , are positive in some months and negative in others, indicating that the prediction errors increase in certain months but decrease in others. Therefore, the evolution of prediction errors shows clear seasonal dependence. In CanESM2 and MPI-ESM-LR, the prediction errors grow rapidly during April–May and July–August, in the late winter/early spring and summer, respectively. In MIROC5, the largest error growth rates occur during January–February and May–July, in winter and early summer, respectively. In CSIRO Mk3.6.0, the prediction errors grow rapidly in February and June–August. Therefore, there are mainly two periods during which the prediction errors increase rapidly in the four models, and they are generally located in late winter/early spring and summer. Referring to the definition of the WPB by Feng et al. (2014b), the WPB phenomenon occurs in the four models when the prediction errors grow most rapidly in winter. We used this as the basis to define the existence of the summer predictability barrier (SPB) in the four models.

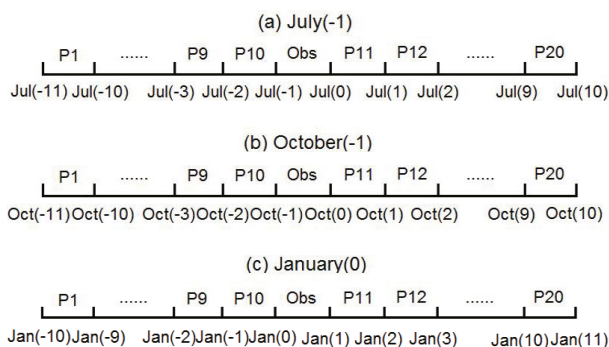


**Fig. 1.** Schematic diagram of the experimental design for one reference year with start months of (a) July(−1), (b) October(−1), and (c) January(0), July(−11), July(−10)... July(10) during the different years on the x-axis indicating the first month of predictions and observations. P1, P2... P20 indicate the 20 predictions for each “observation” with different initial conditions.

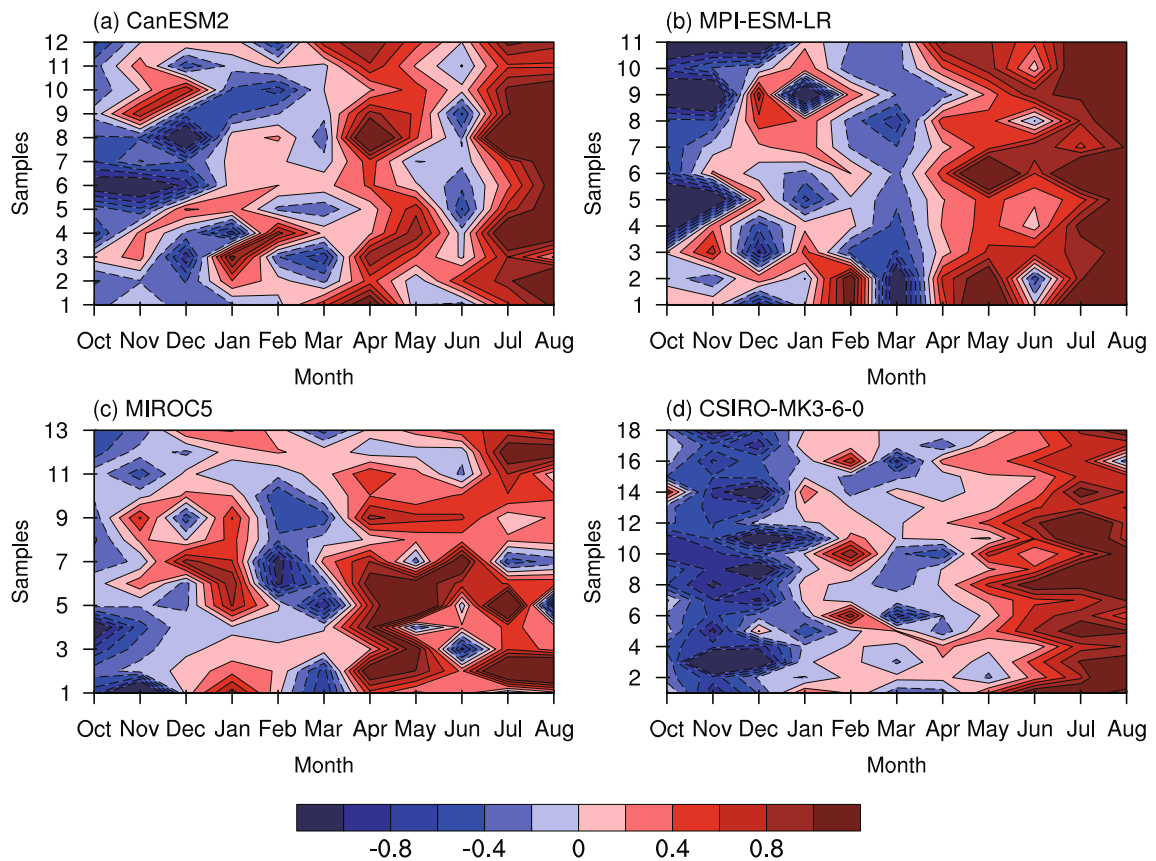


**Fig. 2.** Ensemble mean of the monthly error growth rates for each reference IOD year (units: month<sup>-1</sup>) in models (a) CanESM2, (b) MPI-ESM-LR, (c) MIROC5 and (d) CSIRO Mk3.6.0. The horizontal axes denote the months from October to August. The vertical axes denote the reference IOD events.

By tracing the evolution of prediction errors in each prediction in the four models, it is found that some prediction errors grow fastest in winter or summer and cause a significant WPB or SPB. Conversely, other prediction errors show no season-dependent evolution. As the prediction errors are caused by initial errors only, we inferred that some initial errors could cause a significant WPB or SPB, whereas others could not. Therefore, we selected the initial errors that cause significant predictability barriers, analyzed their spatial patterns, and identified their effects on IOD predictability.

### 3.2. Spatial patterns of initial errors that cause a significant predictability barrier

We selected initial errors that show season-dependent evolution and cause a significant WPB or SPB to identify their dominant spatial patterns. In particular, when prediction errors grow fastest in winter (summer), the corresponding initial errors are considered to yield a significant WPB (SPB). These initial errors are defined as WPB- and SPB-related initial errors, respectively. We then conducted separate empirical orthogonal function (EOF) analyses on the WPB- and SPB-related initial errors. The first EOF mode (i.e., EOF1) describes the dominant spatial patterns of these initial errors. The combination of the EOF1 mode and the corresponding time series (i.e., PC1) indicates that the initial errors can be

divided into two types, with one type similar to the EOF1 mode and the other type as its opposite. Therefore, there are mainly two types of WPB- and SPB-related initial errors. When the individual values of time-series PC1 are positive (negative), the composite of the corresponding WPB-related initial errors is defined as type-1-WPB (type-2-WPB) initial errors. We defined the type-1- and type-2-SPB initial errors in a similar way.

We use CanESM2 as an example to describe the dominant spatial patterns of predictability barrier-related initial errors (Fig. 3). Type-1-WPB initial errors show positive temperature errors in the western Indian Ocean and negative temperature errors in the eastern Indian Ocean. The largest values of the initial errors are concentrated at thermocline depth. Meanwhile, positive temperature errors occur in the subsurface western Pacific Ocean and negative temperature errors in the upper eastern Pacific Ocean. For type-2-WPB initial errors, the spatial pattern of temperature errors in the tropical Indian Ocean is almost opposite to that for type-1-WPB initial errors, whereas the initial errors in the tropical Pacific Ocean are very weak. These results indicate that the initial errors in the tropical Indian Ocean play an important role in causing a significant WPB. In contrast, the initial errors in the tropical Pacific Ocean may have some effect on the occurrence of the WPB; however, this is not a requirement. For

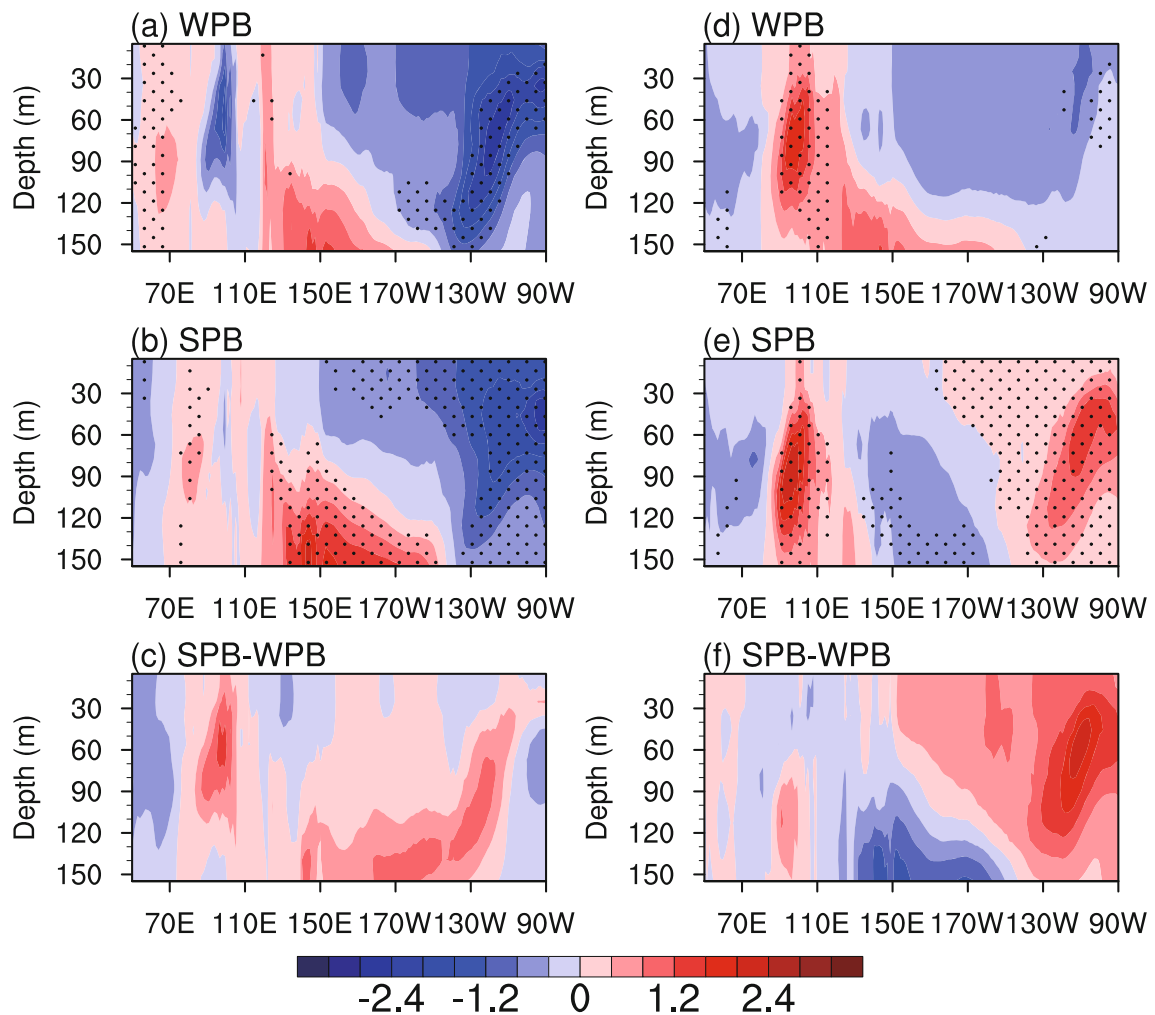


**Fig. 3.** Spatial patterns of the equatorial ( $5^{\circ}\text{S}$ – $5^{\circ}\text{N}$ ) subsurface temperature component of the (a) type-1-WPB initial errors, (b) type-1-SPB initial errors, and (c) the difference between them, in CanESM2 (units:  $^{\circ}\text{C}$ ). Panels (d–f) show the spatial patterns of the type-2-WPB initial errors, type-2-SPB initial errors, and the difference between them, respectively. Dotted areas indicate that the composites of the subsurface temperature errors exceed the 95% significance level, as determined by the  $t$ -test.

the two types of SPB-related initial errors, the temperature errors in the tropical Indian Ocean are weaker, or remain unchanged, compared with those for the WPB-related initial errors. Conversely, the temperature errors in the Pacific Ocean are significantly stronger than those for WPB-related initial errors. The spatial patterns of temperature errors in the Pacific Ocean for the two types of SPB-related initial errors are almost the opposite, with one pole in the subsurface western Pacific Ocean and the other in the upper eastern Pacific Ocean. This indicates that the initial errors in the tropical Pacific Ocean are closely related to the occurrence of the SPB, while the existence of the initial errors in the Indian Ocean is not a requirement.

The major characteristics of the predictability barrier-related initial errors are similar in the other three models (Figs. 4–6). The occurrence of the WPB is closely related to the initial errors in the tropical Indian Ocean, which show a west–east dipole pattern, with the largest values concen-

trated at thermocline depth. These results are consistent with those in previous studies (Feng et al., 2017; Feng and Duan, 2017). The initial errors in the tropical Pacific Ocean may have some effect on the occurrence of the SPB, but are not a requirement. Furthermore, the occurrence of the SPB is most likely caused by initial errors in the tropical Pacific Ocean, with one pole in the subsurface western Pacific Ocean and the other in the upper eastern Pacific Ocean. The presence of initial errors in the tropical Indian Ocean is not a requirement for the occurrence of the SPB.

### 3.3. Physical mechanisms of development for initial errors that cause a significant WPB

We explored why the two types of WPB-related initial errors grow fastest in winter and cause a significant WPB by tracking the evolution of sea temperature and wind anomalies. As the major results are similar between the four models, CanESM2 is taken as an example.

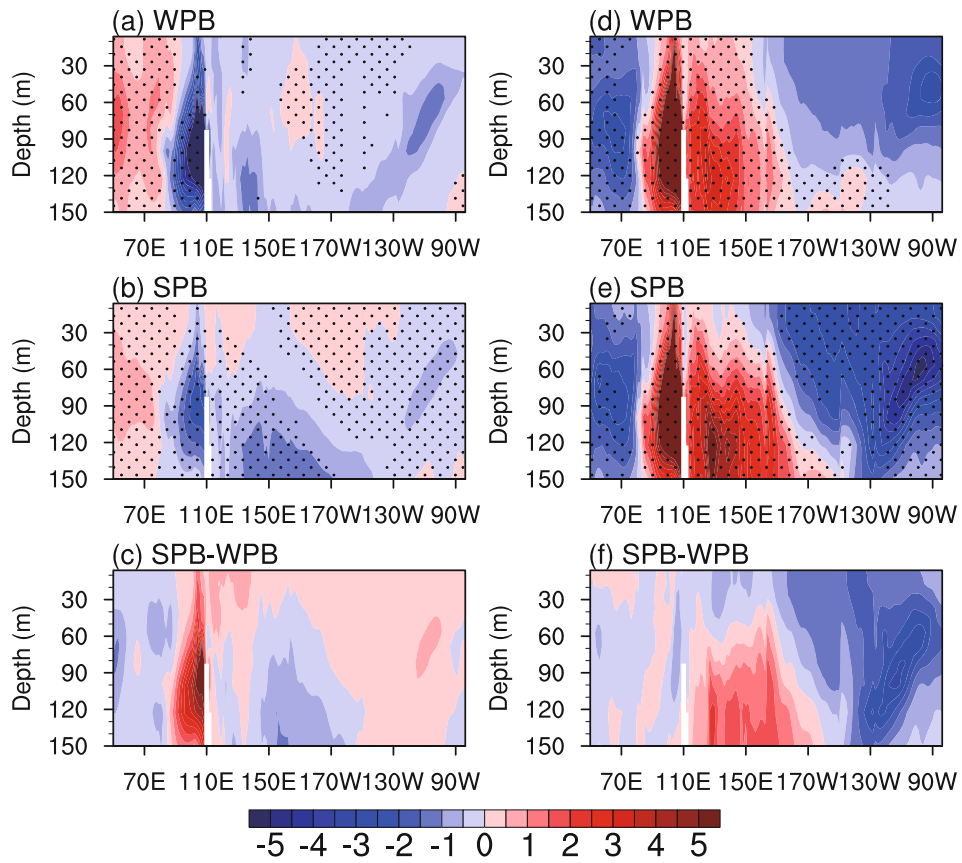


Fig. 4. As in Fig. 3 but for MPI-ESM-LR.

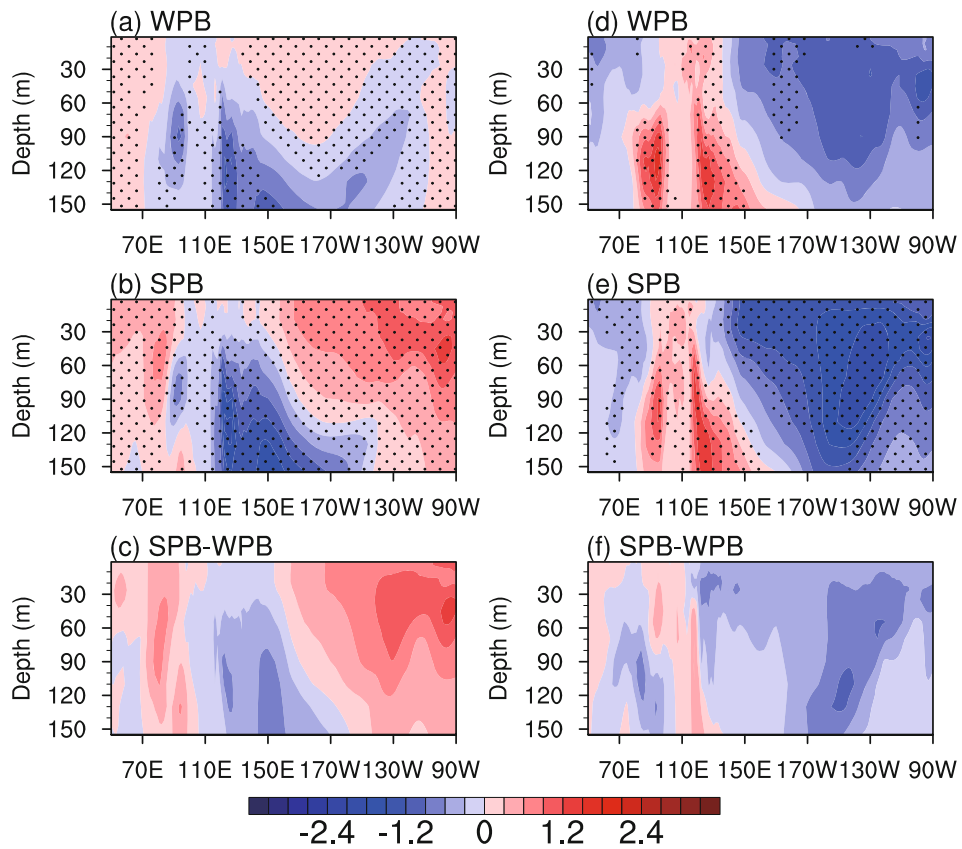


Fig. 5. As in Fig. 3 but for MIROC5.

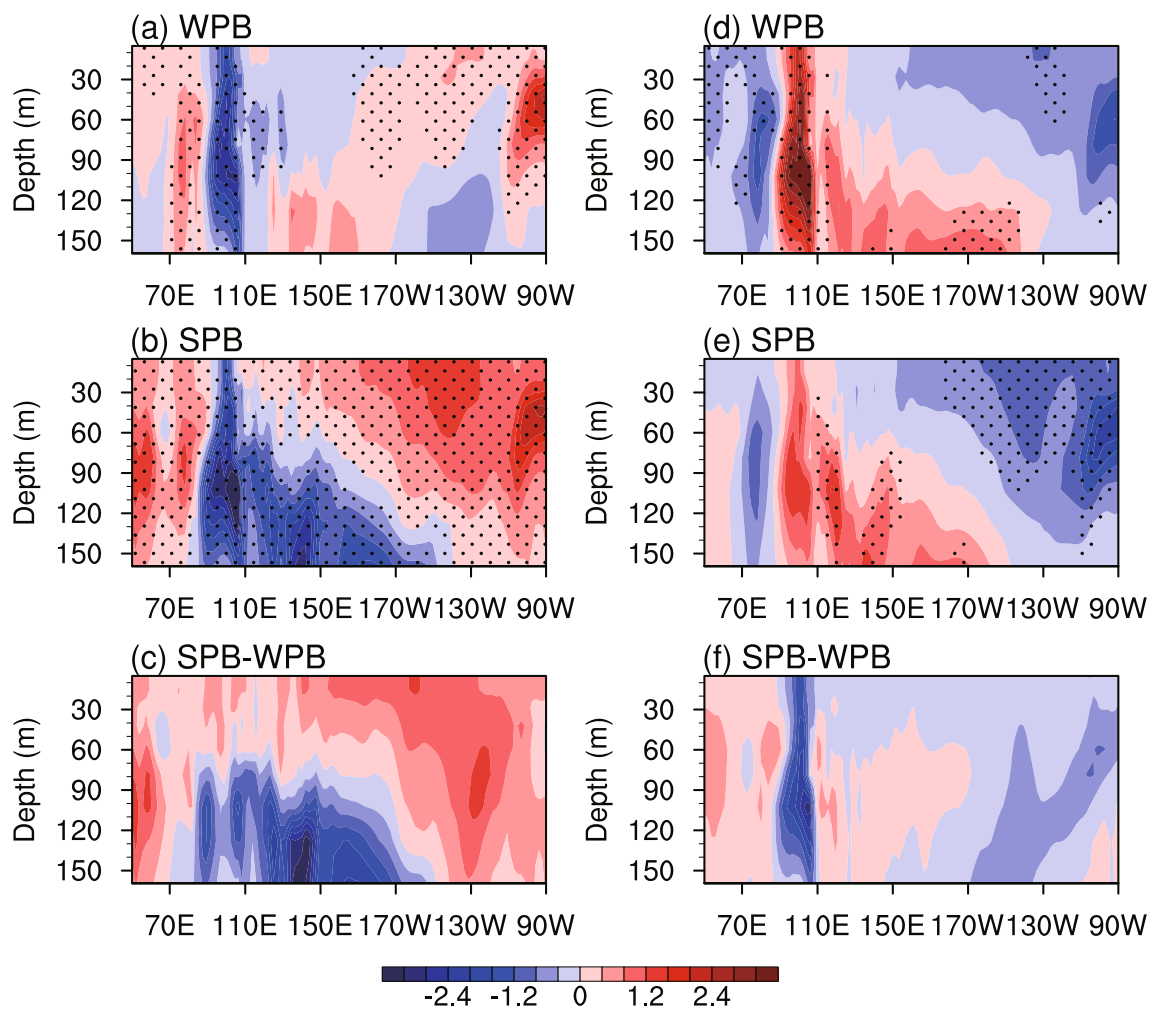
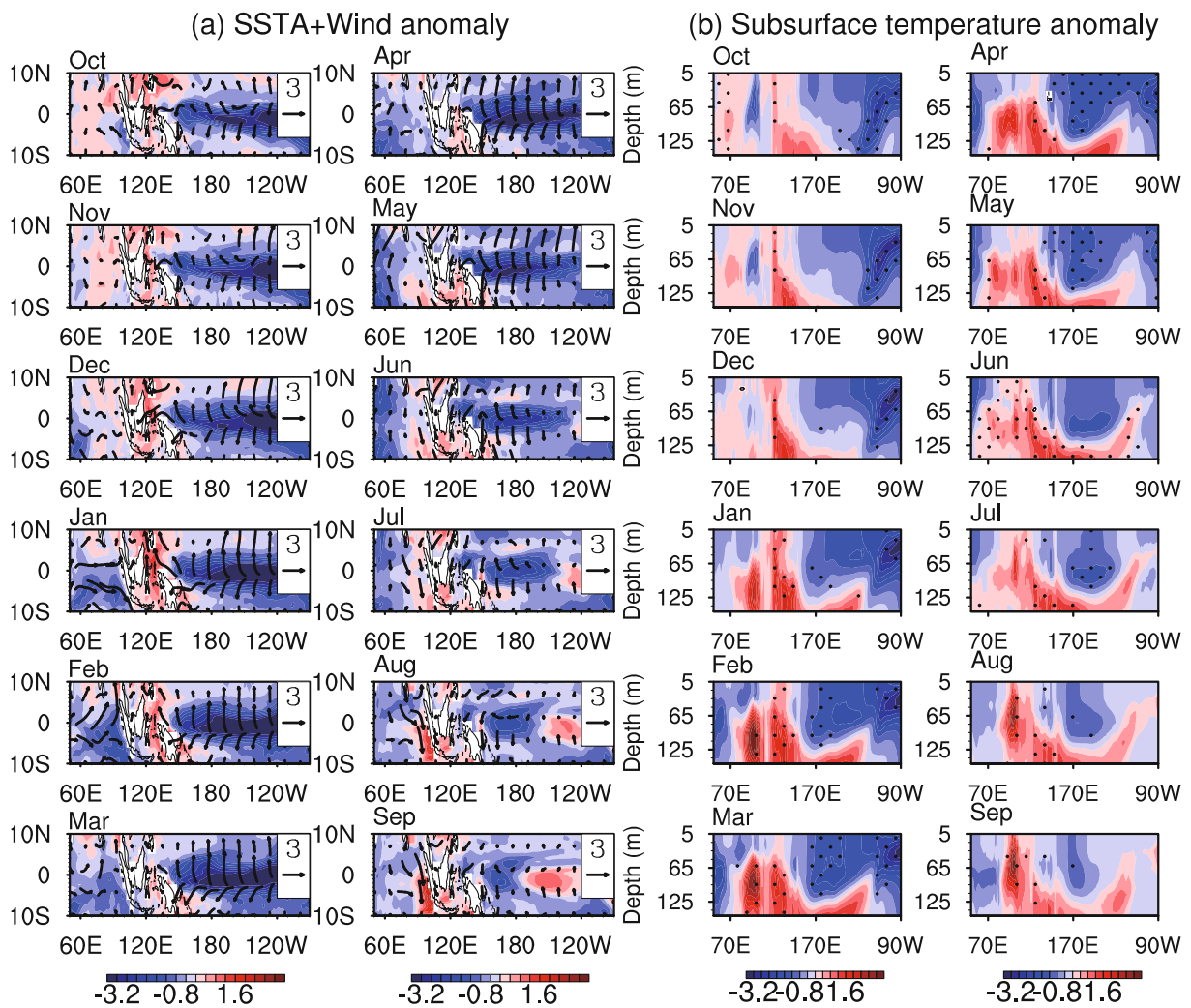


Fig. 6. As in Fig. 3 but for CSIRO Mk3.6.0 model.

When type-1-WPB initial errors are superimposed on the initial temperature field of the “predicted” IOD events (Fig. 7), positive errors in the western Indian Ocean deepen the thermocline and cause downwelling Kelvin waves, which propagate eastward and warm the subsurface eastern Indian Ocean. Meanwhile, the negative errors in the eastern Indian Ocean raise the thermocline and cause upwelling Rossby waves, which propagate westward and cool the subsurface western Indian Ocean. Therefore, several months later, a significant west–east dipole pattern appears in the subsurface ocean, with negative errors in the western Indian Ocean and positive errors in the eastern Indian Ocean. In December–February, the westerly wind anomalies in the tropical Indian Ocean favor the formation of the dipole pattern in the subsurface Indian Ocean by inducing downwelling Kelvin waves and upwelling Rossby waves. Moreover, the westerly wind anomalies have the same wind direction as the climatological wind in the southern Indian Ocean (figure omitted), which increases the total wind speed and suppresses the surface warming in the southeastern Indian Ocean by releasing more latent heat flux (Fig. 8). It is suspected that the westerly wind anomalies in the Indian Ocean likely have a close relationship

with the negative SST errors in the tropical Pacific Ocean, which induce easterly wind anomalies in the tropical Pacific Ocean and modulate the variation of the Walker circulation in the tropical Indian and Pacific oceans (Chen, 2010; Lian et al., 2014; Figure 7). In March–May, the westerly wind anomalies disappear, as well as the suppression effects of latent heat flux errors on the surface warming in the southeastern Indian Ocean (Fig. 8). Because the coupled system in the Indian Ocean is at its weakest in this period and is easily affected by perturbations (Feng et al., 2014a), the SST errors in the Indian Ocean grow rapidly and cause positive SST errors in the eastern Indian Ocean and negative SST errors in the western Indian Ocean, resulting in large prediction errors and a significant WPB.

When the type-2-WPB initial errors are superimposed on the initial field of the reference state IOD events, negative temperature errors appear in the western Indian Ocean, and positive temperature errors occur in the eastern Indian Ocean; whereas, the initial errors in the Pacific Ocean are weak (Fig. 9). In the first half of the prediction year, the sea temperature errors in the tropical Indian Ocean remain almost unchanged (Fig. 9). In winter, the weakest coupled system in the



**Fig. 7.** Evolutions of the SSTA (units:  $^{\circ}\text{C}$ ) and sea surface wind anomaly (units:  $\text{m s}^{-1}$ ) over the tropical Indian and Pacific oceans (left column) and the equatorial ( $5^{\circ}\text{S}$ – $5^{\circ}\text{N}$ ) subsurface temperature anomaly (units:  $^{\circ}\text{C}$ ; right column) for the type-1-WPB initial errors. Dotted areas indicate that the composites of SST and subsurface temperature errors exceed the 95% significance level, as determined by the  $t$ -test.

Indian Ocean favors the rapid growth of perturbations (Feng et al., 2014a). Hence, positive (negative) SST errors develop quickly in the eastern (western) Indian Ocean, and are further amplified by Bjerknes feedback, causing large prediction errors in winter and resulting in a significant WPB.

Based on the above discussion, the occurrence of the WPB has a close relationship with the dipole pattern initial errors in the tropical Indian Ocean. Although initial errors in the tropical Pacific Ocean have some influence on causing a WPB, this is not a requirement. In addition to the spatial patterns of initial errors, the climatological conditions in winter in the Indian Ocean also play an important role in causing a significant WPB.

### 3.4. Physical mechanisms of development of initial errors that cause a significant SPB

The occurrence of the SPB is mainly caused by initial errors in the tropical Pacific Ocean. In this section, in consideration of the similar results between the four models, we

only use CanESM2 as an example, for simplicity, to explore how these initial errors develop and cause a significant SPB.

When the type-1-SPB initial errors are superimposed on the initial field of the reference state IOD events, there are positive temperature errors in the subsurface western Pacific Ocean and negative temperature errors in the upper eastern Pacific Ocean; the initial errors in the tropical Indian Ocean are weak (Fig. 10). The SST errors in the tropical Pacific Ocean show a La Niña-like development (Duan and Hu, 2016). In response to the negative SST errors in the tropical Pacific Ocean, strong easterly wind anomalies occur at the equator, which further induce westerly wind anomalies in the tropical Indian Ocean by modulating the variation of the Walker circulation in the tropical oceans (Chen, 2010; Lian et al., 2014). On the one hand, the westerly wind anomalies in the tropical Indian Ocean induce eastward downwelling Kelvin waves and westward upwelling Rossby waves, which cause positive (negative) temperature errors in the subsurface eastern (western) Indian Ocean. On the other hand, the west-

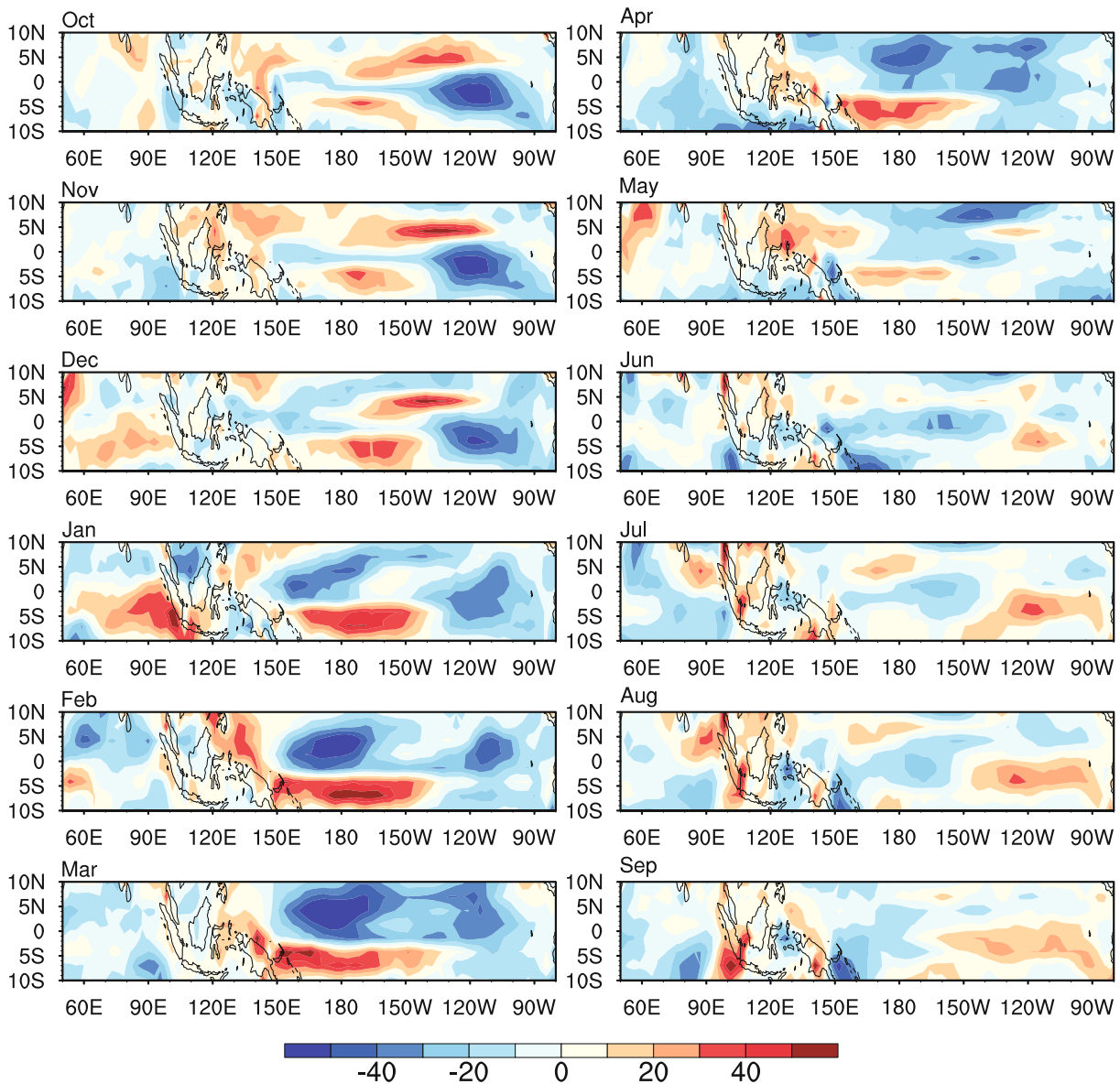


**Fig. 8.** Evolutions of latent heat flux errors (units:  $W m^{-2}$ ) over the tropical Indian and Pacific oceans for the type-1-WPB initial errors in CanESM2.

erly wind anomalies have the same wind direction as the climatological wind, particularly in the southern Indian Ocean, which increases the total wind speed and cools the sea surface water there by releasing more latent heat flux (Fig. 11). This results in basin-wide cooling for several months. When the climatological wind direction reverses in summer, the westerly wind anomalies in the eastern Indian Ocean decrease the total wind speed and in turn warm the sea surface water by decreasing the latent heat flux release (Fig. 11). Then, positive (negative) SST errors in the eastern (western) Indian Ocean further grow rapidly under the Bjerknes positive feedback. This causes large prediction errors in July and August, ultimately resulting in a significant SPB.

When we superimpose the type-2-SPB initial errors on the initial state of the reference state IOD events, temperature errors with a west–east dipole pattern appear in the In-

dian Ocean. Meanwhile, negative (positive) temperature errors appear in the subsurface western (upper eastern) Pacific Ocean (Fig. 12). The initial errors superimposed in the Indian Ocean decay rapidly over the first few months. However, the evolution of SST errors in the tropical Pacific Ocean initially features a period similar to an El Niño decaying phase, subsequently exhibiting a transition to a cold phase and evolving into a La Niña–like mode (Duan and Hu, 2016). Corresponding to the positive SST errors in the Pacific Ocean in the first half of the prediction year, weak westerly wind anomalies appear at the equator, which further induces weak easterly wind anomalies in the Indian Ocean by modulating the variation of Walker circulation in the tropical oceans (Chen, 2010; Lian et al., 2014). Similarly, the westerly wind anomalies in the Indian Ocean in the second half of the prediction year are closely linked with the negative SST errors in the Pacific

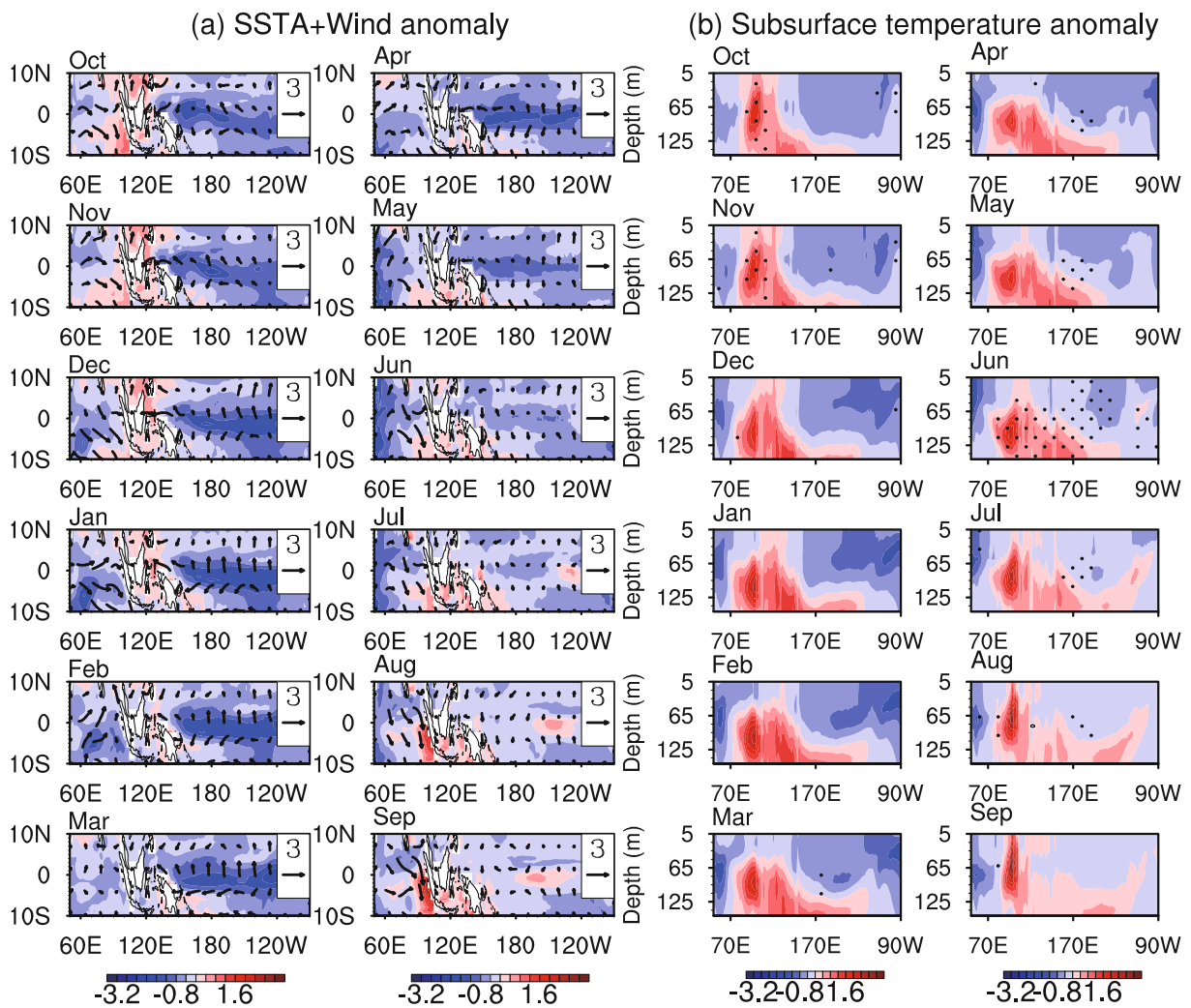


Fig. 9. As in Fig. 7 but for the type-2-WPB initial errors.

Ocean. This westerly wind anomalies in the Indian Ocean induce downwelling Kelvin waves in the second half of the prediction year, which pile up warm water in the subsurface eastern Indian Ocean. The cold water is supplemented in the subsurface western Indian Ocean. Moreover, the westerly wind anomalies first cool the sea surface water in the southern Indian Ocean, because of the same wind direction as the climatological wind, which increases the total wind speed and releases more latent heat flux (i.e., April in Fig. 13). In summer, the climatological wind reverses to a southeast wind, especially in the southern Indian Ocean. Therefore, the westerly wind anomalies in turn warm the sea surface water in the southeastern Indian Ocean (Fig. 13). With the help of positive Bjerknes feedback, the positive SST errors grow fastest in the eastern Indian Ocean and cause a significant west–east dipole pattern in the Indian Ocean. The prediction errors grow fastest in July and August and result in a significant SPB.

Based on the above discussion, the occurrence of the SPB is mainly caused by the initial errors in the tropical Pacific Ocean. In addition, the reversal of the climatological wind

direction also plays a key role in causing a significant SPB. Therefore, the occurrence of the SPB is closely related with the spatial patterns of the initial errors and the climatological conditions.

#### 4. Implications

We demonstrated in section 3 that the initial errors due to the sparse availability of observational data in the tropical Indian and Pacific oceans cause rapid growth of the prediction errors in winter and summer, resulting in a significant WPB and SPB. The existence of the WPB and the SPB greatly limits the forecast skill of positive IOD events at a lead time of one season (Luo et al., 2007). Therefore, more observations are needed to provide a more accurate initial field and improve the forecast skill of positive IOD events. However, collecting a lot of observations in the Indian and Pacific oceans is costly and will never be dense enough to fully cover the vast tropical oceans. A targeted observation strategy has been suggested (Snyder, 1996; Mu et al., 2014) where, to better forecast an event at a future time (i.e., the verification time)

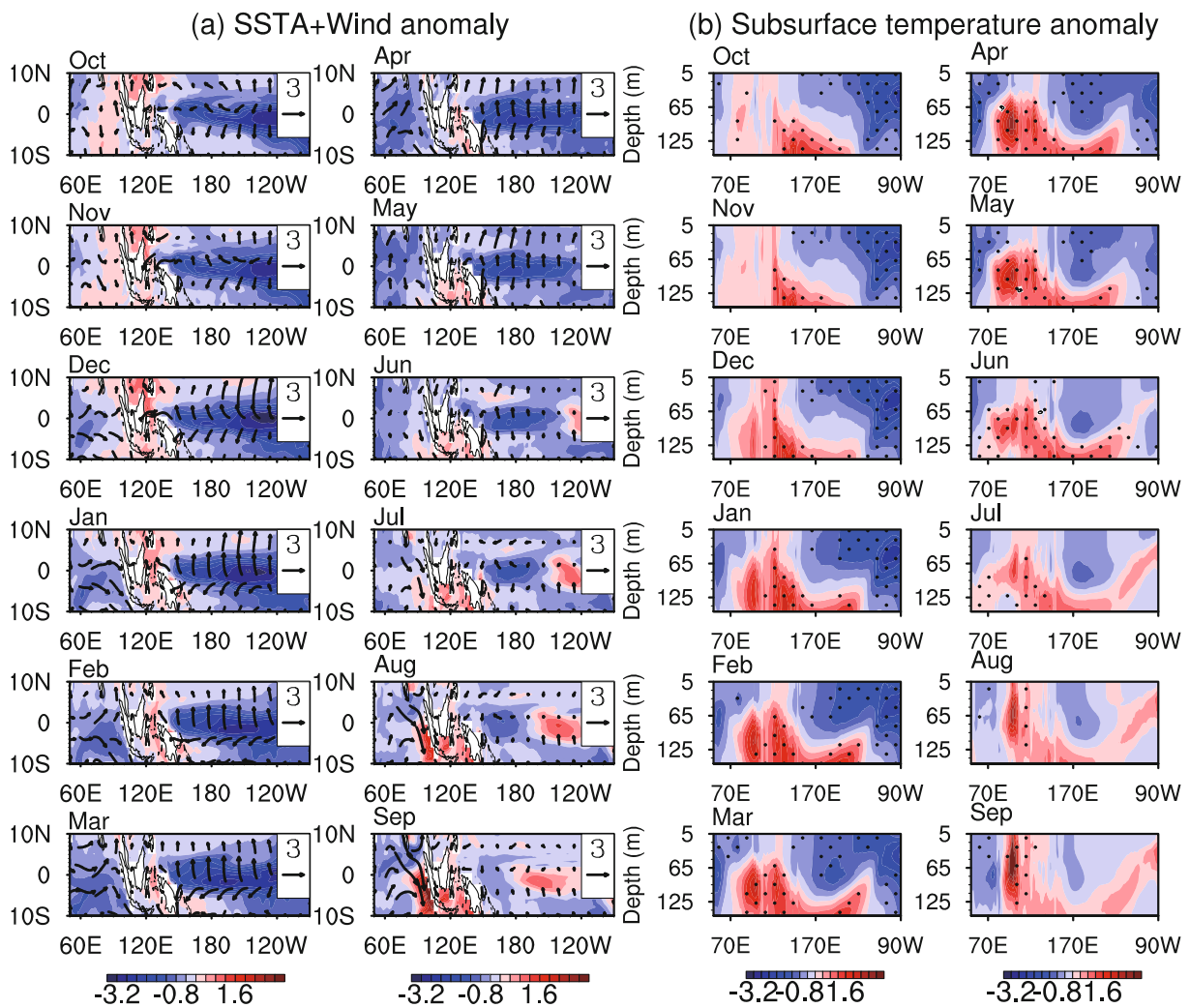


Fig. 10. As in Fig. 7 but for the type-1-SPB initial errors.

in an area of interest (i.e., the verification area), observations need to be carried out in certain key areas (i.e., the sensitive areas) at the target time. It is assumed that the observations in these sensitive areas will reduce the prediction errors to a larger degree than the same number of observations in other areas. The key to this strategy is to explore the sensitive areas for targeted observations.

It has been demonstrated that the WPB is mainly caused by initial errors in the tropical Indian Ocean, which present a west–east dipole pattern with the largest values located at thermocline depth. By tracing the evolution of sea temperature and wind anomalies, we found that the initial errors in these large-value areas contribute greatly to the large prediction errors in winter. That is, the prediction errors in winter may be highly sensitive to initial errors in these areas. These areas are therefore most likely the key locations (i.e., sensitive areas) where to obtain targeted observations to advance beyond the WPB. For the two types of SPB-related initial errors, the largest values are located in the subsurface western Pacific Ocean and the upper eastern Pacific Ocean. Similarly, the initial errors in these large-value areas contribute

greatly to the prediction errors in summer. These two areas are likely the key areas where to obtain targeted observations to advance beyond the SPB.

Based on the above discussion, we have identified four areas that are likely to be the sensitive areas of positive IOD events where to obtain targeted observations. If observations are obtained over these areas preferentially and assimilated into the initial field, a more accurate initial field will be obtained, which will greatly improve the forecast skill of IOD events. However, Observing System Simulation Experiments (OSSEs) and Observing System Experiments (OSEs) are still needed in future work to further verify the effectiveness of these sensitive areas in improving the forecast skill of positive IOD events.

### 5. Summary

The IOD is an important ocean–atmosphere coupled phenomenon in the tropical Indian Ocean, which has significant climatic effects on surrounding and more distant regions. By analyzing the output of the PI control runs of four models

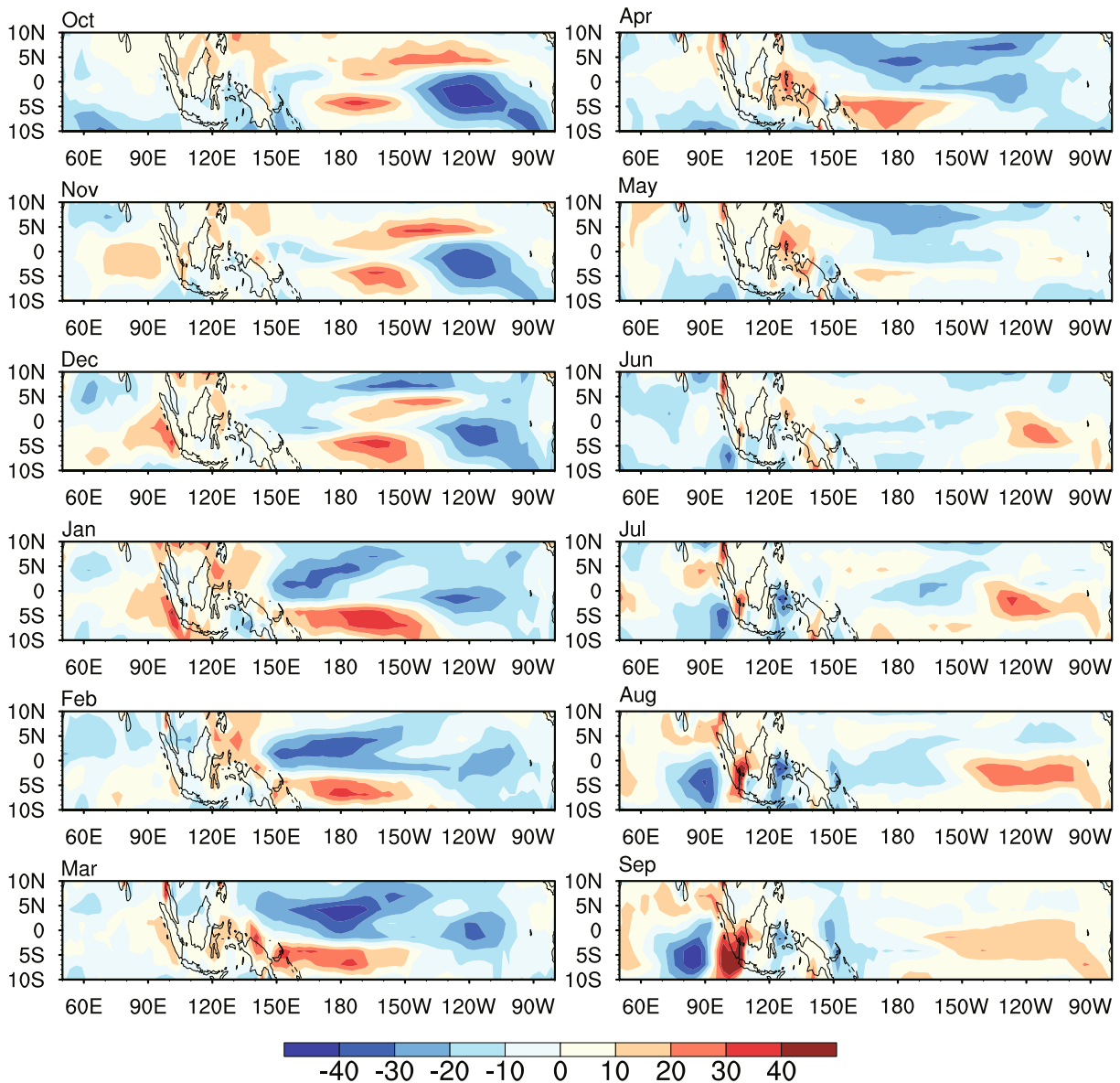


Fig. 11. As in Fig. 8 but for the type-1-SPB initial errors in CanESM2.

within CMIP5, we have demonstrated that the prediction errors grow fastest in winter or summer, and cause a significant WPB or SPB phenomenon. As the forcing in the PI control runs is time-invariant, the prediction errors here are only caused by initial errors.

The dominant spatial patterns of initial errors that are most likely to cause a significant WPB or SPB have been identified. There are two types of WPB-related initial errors in the four models. Type-1-WPB initial errors show a west–east dipole pattern in the tropical Indian Ocean, and the largest values of the initial errors are concentrated at thermocline depth. The type-2-WPB initial errors in the Indian Ocean are almost opposite to the type-1-WPB initial errors. Although there are some temperature errors in the tropical Pacific Ocean in the type-1-WPB initial errors, it is not a requirement for the occurrence of the WPB. Similarly, there are two types of SPB-related initial errors. For type-1-SPB initial

errors, there are positive temperature errors in the subsurface western Pacific Ocean and negative temperature errors in the upper eastern Pacific Ocean. For the type-2-SPB initial errors, temperature errors in the tropical Pacific Ocean are almost opposite to those in the type-1-SPB initial errors. In contrast, temperature errors in the Indian Ocean are weaker, or remain unchanged, compared with those for the WPB-related initial errors. This indicates that the initial errors in the tropical Indian Ocean may not be important to the occurrence of the SPB, and that the initial errors in the tropical Pacific Ocean play a key role in causing a significant SPB.

Furthermore, by analyzing the evolution of sea temperature and wind anomalies, we explored the physical mechanisms responsible for the development of the initial errors that cause a significant WPB or SPB. Due to the similar results among the four models, the CanESM2 model was taken as an example in the discussions. For the type-1-WPB ini-

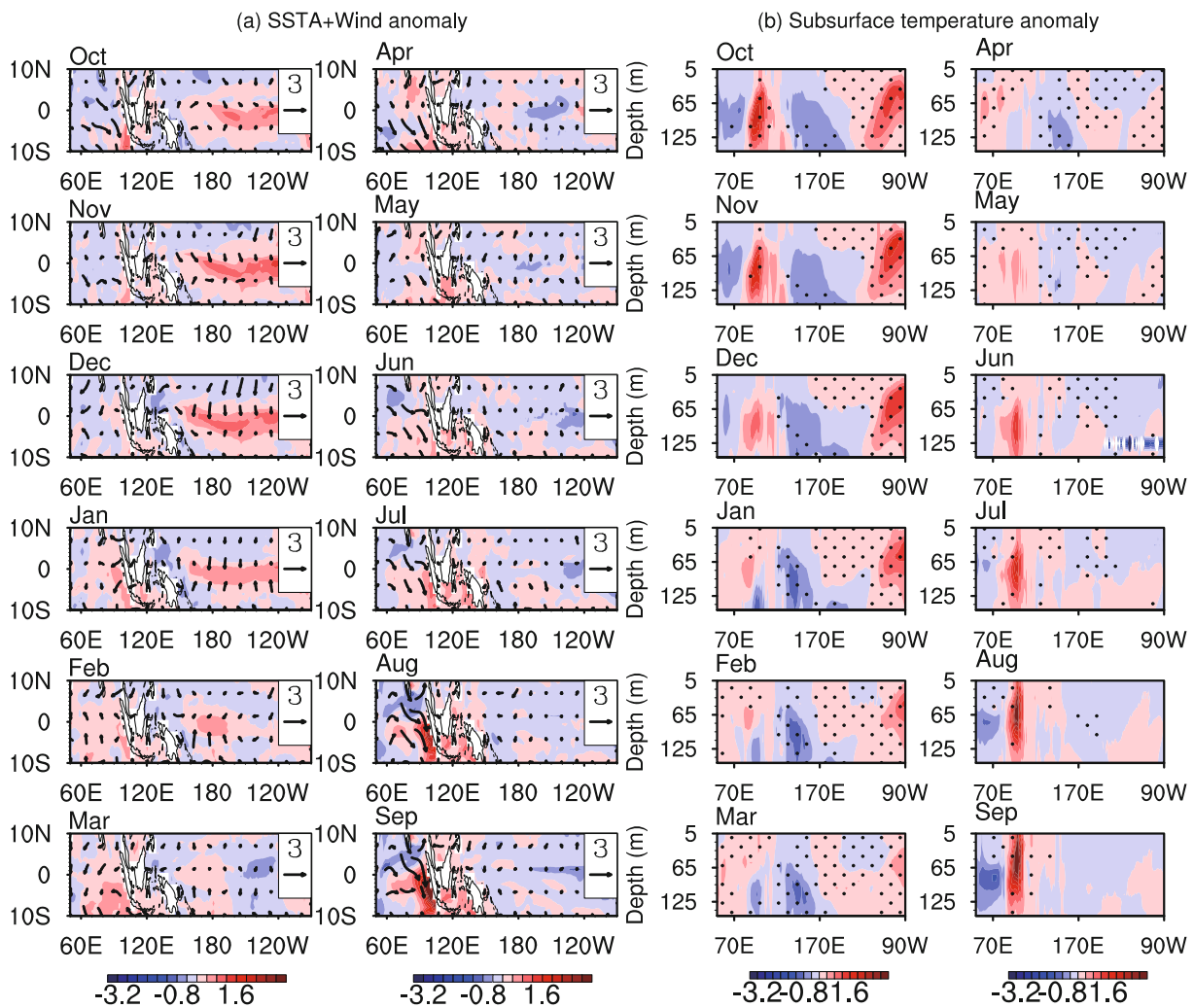


Fig. 12. As in Fig. 7 but for the type-2-SPB initial errors.

tial errors, the temperature errors develop under the effects of ocean waves, which create negative errors in the subsurface western Indian Ocean and positive errors in the subsurface eastern Indian Ocean. The westerly wind anomalies in the tropical Indian Ocean, which are probably induced by the negative temperature errors in the tropical Pacific Ocean by modulating the Walker circulation in tropical oceans, also help to form the dipole pattern. Moreover, the westerly wind anomalies cool the sea surface water and suppress the warming in the eastern Indian Ocean by releasing more latent heat flux. In winter, the westerly wind anomalies disappear. The coupled system is at its weakest during this period, which favors the fastest growth of the perturbations. Therefore, the SST errors grow most rapidly in the Indian Ocean and a clear west–east dipole pattern of SST errors appears in winter. This indicates large prediction errors and the occurrence of a significant WPB. For the type-2-WPB initial errors, the temperature errors in the Indian Ocean remain unchanged in the first few months. In winter, because of the coupled system being in its weakest state, the SST errors grow fastest in the Indian Ocean, resulting in a significant west–east dipole pattern, and

ultimately a significant WPB. In conclusion, in addition to the spatial patterns of initial errors in the Indian Ocean, the climatological conditions in winter are also an important factor in causing the WPB.

For the two types of SPB-related initial errors, the initial errors in the Indian Ocean are weak or decay rapidly over the first few months. Conversely, for the type-1-SPB initial errors, the prediction errors in Pacific Ocean undergo a period similar to the El Niño decaying phase and then a La Niña development phase. For the type-2-SPB initial errors, the prediction errors in the Pacific Ocean feature La Niña-like development. Both types of SPB-related initial errors cause negative SST errors in the tropical Pacific Ocean in the second half of the prediction year. These negative SST errors induce easterly wind anomalies in the Pacific Ocean and then westerly wind anomalies in the Indian Ocean by modulating the Walker circulation in the tropical oceans. On the one hand, the westerly wind anomalies pile up warm water in the subsurface eastern Indian Ocean and, as a result, cold water is supplemented in the subsurface western Indian Ocean. On the other hand, due to the same wind direction of the cli-

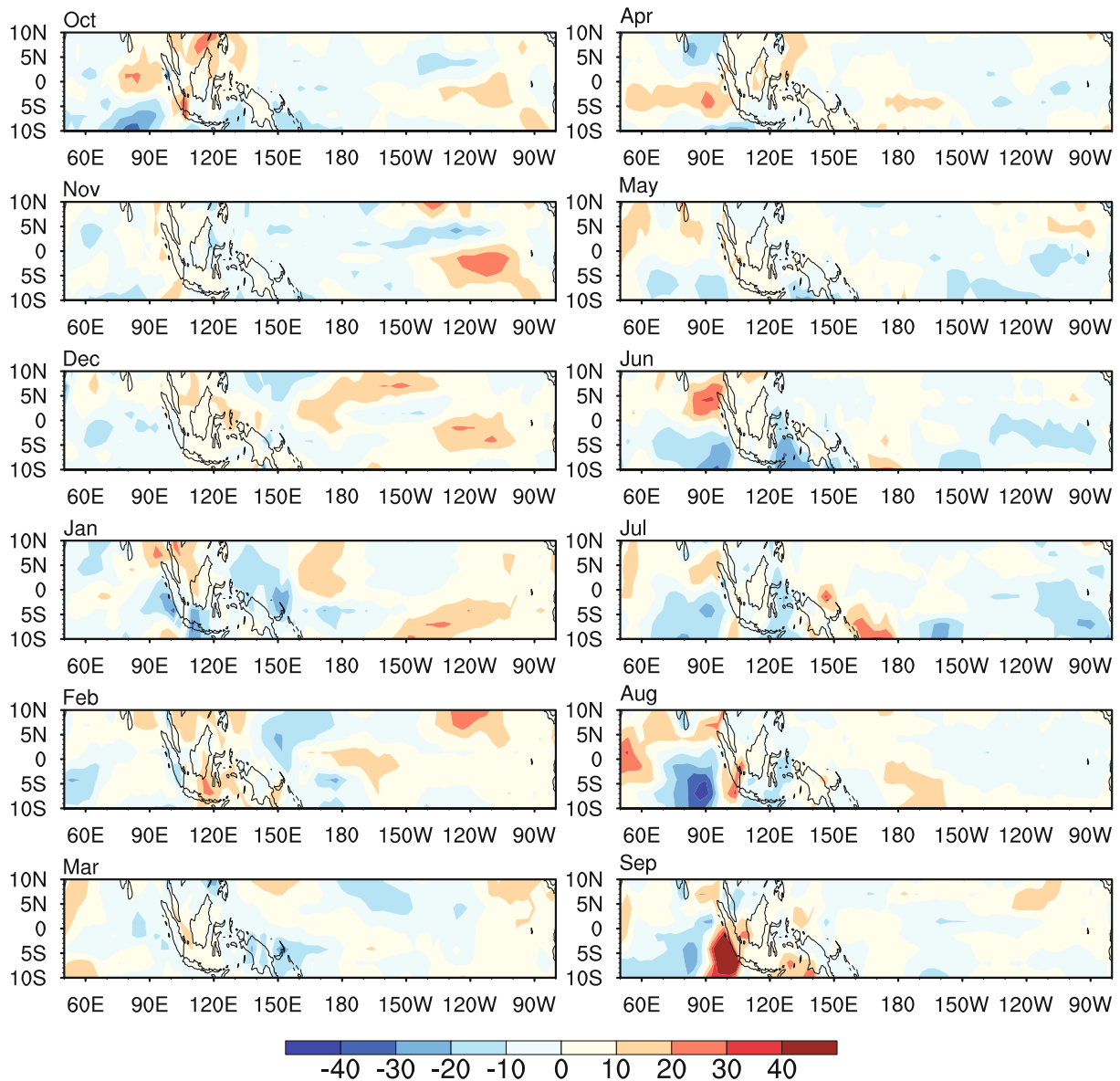


Fig. 13. As in Fig. 8 but for the type-2-SPB initial errors in CanESM2.

matological wind, the westerly wind anomalies cool the sea surface water and suppress the warming in the eastern Indian Ocean by releasing more latent heat flux. However, in summer, when the climatological wind reverses direction, the westerly wind anomalies in turn warm the sea surface water in the eastern Indian Ocean and cause a significant west–east dipole pattern of SST errors. This indicates the fast growth of prediction errors in summer, causing a significant SPB. The occurrence of the SPB is closely linked with the spatial patterns of the initial errors in the tropical Pacific Ocean and the climatological conditions in summer.

It has been found that CanESM2 and CSIRO-Mk3.6.0 simulate an excessively large IOD amplitude with an overly strong Bjerknes feedback, as determined by an evaluation of IOD performance in 14 CMIP5 models. In contrast, MPI-ESM-LR and MIROC5 simulate an IOD magnitude close to observations, and the Bjerknes feedback in these models is

appropriate. As suggested in this study, the WPB- and SPB-related initial errors grow rapidly under Bjerknes feedback and lead to predictability barriers, meaning the overly strong Bjerknes feedback in CanESM2 and CSIRO-Mk3.6.0 may cause overestimated predictability barriers.

The largest values of WPB- and SPB-related initial errors are mainly concentrated within a few areas. By tracing the evolution of sea temperature and wind anomalies, we found that initial errors in these areas contribute greatly to the prediction errors in winter or summer. That is, the prediction errors may be highly sensitive to the initial errors over these areas, which are likely the sensitive areas of positive IOD events for targeted observations. If we carry out intensive observations over these areas and assimilate the observations to obtain a more accurate initial field, the prediction errors will likely be largely reduced and the forecast skill greatly improved. However, OSSEs and OSEs are needed in future

work to further verify the effectiveness of these sensitive areas in improving the forecast skill of positive IOD events.

Based on the above discussion, the effects of initial errors in the tropical Indian and Pacific oceans on IOD predictions have been identified, which reflects the close relationship of SST variabilities in these oceans. ENSO, as the dominant phenomenon in the tropical Pacific Ocean, might also have some effects on the WPB and SPB. In addition to the Pacific Ocean, the Atlantic and Arctic oceans also interact with the Indian Ocean, and hence initial errors in these oceans probably have an impact on IOD predictions. So, are there any sensitive areas of positive IOD events for targeted observations in other oceans aside from those identified in this study? We have only considered initial sea temperature errors; however, the possible roles of other atmospheric and oceanic variables on IOD predictions should be studied, and whether these variables can provide information to identify sensitive areas for targeted observations. Furthermore, sensitivity experiments using a global coupled ocean–atmosphere general circulation model should be conducted to better understand the influence of the initial temperature errors in the Indian and Pacific oceans on the IOD predictions. Therefore, work remains to be done on targeted observations of positive IOD events, which is expected to greatly improve the forecast skill of IOD events.

**Acknowledgements.** This work was jointly sponsored by the National Natural Science Foundation of China (Grant Nos. 41506032 and 41530961), and the National Programme on Global Change and Air–Sea Interaction (Grant No. GASI-IPOVAI-06).

## REFERENCES

- Annamalai, H., and R. Murtugudde, 2004: Role of the Indian Ocean in regional climate variability. *Earth Climate: The Ocean–Atmosphere Interaction*, Washington, AGU, 213–246.
- Ansell, T., C. J. C. Reason, and G. Meyers, 2000: Variability in the tropical southeast Indian Ocean and links with southeast Australian winter rainfall. *Geophys. Res. Lett.*, **27**, 3977–3980, <https://doi.org/10.1029/2000GL011856>.
- Ashok, K., Z. Y. Guan, and T. Yamagata, 2001: Impact of the Indian Ocean dipole on the relationship between the Indian monsoon rainfall and ENSO. *Geophys. Res. Lett.*, **28**, 4499–4502, <https://doi.org/10.1029/2001GL013294>.
- Ashok, K., Z. Y. Guan, and T. Yamagata, 2003: Influence of the Indian Ocean dipole on the Australian winter rainfall. *Geophys. Res. Lett.*, **30**(15), 1821, <https://doi.org/10.1029/2003GL017926>.
- Behera, S. K., J. J. Luo, S. Masson, S. A. Rao, H. Sakuma, and T. Yamagata, 2006: A CGCM study on the interaction between IOD and ENSO. *J. Climate*, **19**(9), 1688–1705, <https://doi.org/10.1175/JCLI3797.1>.
- Behera, S. K., J.-J. Luo, S. Masson, P. Delecluse, S. Gualdi, A. Navarra, and T. Yamagata, 2005: Paramount impact of the Indian Ocean dipole on the East African short rains: A CGCM study. *J. Climate*, **18**, 4514–4530, <https://doi.org/10.1175/JCLI3541.1>.
- Birkett, C., R. Murtugudde, and T. Allan, 1999: Indian Ocean climate event brings floods to East Africa’s lakes and the Sudd Marsh. *Geophys. Res. Lett.*, **26**, 1031–1034, <https://doi.org/10.1029/1999GL900165>.
- Cai, W. J., and T. Cowan, 2013: Why is the amplitude of the Indian Ocean Dipole overly large in CMIP3 and CMIP5 climate models? *Geophys. Res. Lett.*, **40**, 1200–1205, <https://doi.org/10.1002/grl.50208>.
- Cai, W. J., H. H. Hendon, and G. Meyers, 2005: Indian Ocean dipolelike variability in the CSIRO Mark 3 coupled climate model. *J. Climate*, **18**, 1449–1468, <https://doi.org/10.1175/JCLI3332.1>.
- Cai, W. J., T. Cowan, and A. Sullivan, 2009: Recent unprecedented skewness towards positive Indian Ocean Dipole occurrences and its impact on Australian rainfall. *Geophys. Res. Lett.*, **36**, L11705, <https://doi.org/10.1029/2009GL037604>.
- Chen, D., 2010: Indo-Pacific tripole: An intrinsic mode of tropical climate variability. *Advances in Geosciences*, **24**, 1–18, [https://doi.org/10.1142/9789814355535\\_0001](https://doi.org/10.1142/9789814355535_0001).
- Clark, C. O., P. J. Webster, and J. E. Cole, 2003: Interdecadal variability of the relationship between the Indian Ocean zonal mode and East African coastal rainfall anomalies. *J. Climate*, **16**, 548–554, [https://doi.org/10.1175/1520-0442\(2003\)016<0548:IVOTRB>2.0.CO;2](https://doi.org/10.1175/1520-0442(2003)016<0548:IVOTRB>2.0.CO;2).
- Duan, W. S., and M. Mu, 2006: Investigating decadal variability of El Niño–Southern Oscillation asymmetry by conditional nonlinear optimal perturbation. *J. Geophys. Res.*, **111**(C7), C07015, <https://doi.org/10.1029/2005JC003458>.
- Duan, W. S., and J. Y. Hu, 2016: The initial errors that induce a significant “spring predictability barrier” for El Niño events and their implications for target observation: Results from an earth system model. *Climate Dyn.*, **46**, 3599–3615, <https://doi.org/10.1007/s00382-015-2789-5>.
- Duan, W. S., X. C. Liu, K. Y. Zhu, and M. Mu, 2009: Exploring the initial errors that cause a significant “spring predictability barrier” for El Niño events. *J. Geophys. Res.*, **114**(C4), C04022, <https://doi.org/10.1029/2008JC004925>.
- Feng, R., and W. S. Duan, 2017: IOD-related optimal initial errors and optimal precursors for IOD predictions from reanalysis data. *Science China Earth Sciences*, **60**, 156–172, <https://doi.org/10.1007/s11430-016-0103-9>.
- Feng, R., M. Mu, and W. S. Duan, 2014a: Study on the “winter persistence barrier” of Indian Ocean dipole events using observation data and CMIP5 model outputs. *Theor. Appl. Climatol.*, **118**(3), 523–534, <https://doi.org/10.1007/s00704-013-1083-x>.
- Feng, R., W. S. Duan, and M. Mu, 2014b: The “winter predictability barrier” for IOD events and its error growth dynamics: Results from a fully coupled GCM. *J. Geophys. Res.*, **119**, 8688–8708, <https://doi.org/10.1002/2014JC010473>.
- Feng, R., W. S. Duan, and M. Mu, 2017: Estimating observing locations for advancing beyond the winter predictability barrier of Indian Ocean dipole event predictions. *Climate Dyn.*, **48**, 1173–1185, <https://doi.org/10.1007/s00382-016-3134-3>.
- Guan, Z. Y., and T. Yamagata, 2003: The unusual summer of 1994 in East Asia: IOD teleconnections. *Geophys. Res. Lett.*, **30**(10), 1544, <https://doi.org/10.1029/2002GL016831>.
- Han, W. Q., W. T. Liu, and J. L. Lin, 2006: Impact of atmospheric submonthly oscillations on sea surface temperature of the tropical Indian Ocean. *Geophys. Res. Lett.*, **33**, L03609, <https://doi.org/10.1029/2005GL025082>.
- Jin, F. F., 1997: An equatorial ocean recharge paradigm for ENSO. Part I: Conceptual model. *J. Atmos. Sci.*, **54**(7), 811–829, [https://doi.org/10.1175/1520-0469\(1997\)054<0811:](https://doi.org/10.1175/1520-0469(1997)054<0811:)

AEORPF>2.0.CO;2.

- Jourdain, N. C., A. S. Gupta, A. S. Taschetto, C. C. Ummerhofer, A. F. Moise, and K. Ashok, 2013: The Indo-Australian monsoon and its relationship to ENSO and IOD in reanalysis data and the CMIP3/CMIP5 simulations. *Climate Dyn.*, **41**, 3073–3102, <https://doi.org/10.1007/s00382-013-1676-1>.
- Krishnamurthy, V., and B. P. Kirtman, 2003: Variability of the Indian Ocean: Relation to monsoon and ENSO. *Quart. J. Roy. Meteor. Soc.*, **129**(590), 1623–1646, <https://doi.org/10.1256/qj.01.166>.
- Lau, N.-C., and M. J. Nath, 2004: Coupled GCM simulation of atmosphere–ocean variability associated with zonally asymmetric SST changes in the tropical Indian Ocean. *J. Climate*, **17**(2), 245–265, [https://doi.org/10.1175/1520-0442\(2004\)017<0245:CGSOAV>2.0.CO;2](https://doi.org/10.1175/1520-0442(2004)017<0245:CGSOAV>2.0.CO;2).
- Lee, T., I. Fukumori, and D. Menemenlis, Z. F. Xing, and L.-L. Fu, 2002: Effects of the Indonesian Throughflow on the Pacific and Indian Oceans. *J. Phys. Oceanogr.*, **32**, 1404–1429, [https://doi.org/10.1175/1520-0485\(2002\)032<1404:EOTITO>2.0.CO;2](https://doi.org/10.1175/1520-0485(2002)032<1404:EOTITO>2.0.CO;2).
- Li, G., S. P. Xie, and Y. Du, 2015: Monsoon-induced biases of climate models over the tropical Indian Ocean. *J. Climate*, **28**, 3058–3072, <https://doi.org/10.1175/JCLI-D-14-00740.1>.
- Li, T., Y. S. Zhang, E. Lu, and D. L. Wang, 2002: Relative role of dynamic and thermodynamic processes in the development of the Indian Ocean dipole: An OGCM diagnosis. *Geophys. Res. Lett.*, **29**(23), 25-1–25-4, <https://doi.org/10.1029/2002GL015789>.
- Li, T., B. Wang, C.-P. Chang, and Y. S. Zhang, 2003: A theory for the Indian Ocean dipole–zonal mode. *J. Atmos. Sci.*, **60**(17), 2119–2135, [https://doi.org/10.1175/1520-0469\(2003\)060<2119:ATFTIO>2.0.CO;2](https://doi.org/10.1175/1520-0469(2003)060<2119:ATFTIO>2.0.CO;2).
- Lian, T., D. K. Chen, Y. M. Tang, and B. G. Jin, 2014: A theoretical investigation of the tropical Indo-Pacific tripole mode. *Science China Earth Sciences*, **57**, 174–188, <https://doi.org/10.1007/s11430-013-4762-7>.
- Liu, L., S. P. Xie, X. T. Zheng, T. Li, Y. Du, G. Huang, and W. D. Yu, 2014: Indian Ocean variability in the CMIP5 multi-model ensemble: The zonal dipole mode. *Climate Dyn.*, **43**, 1715–1730, <https://doi.org/10.1007/s00382-013-2000-9>.
- Loschnigg, J., G. A. Meehl, P. J. Webster, J. M. Arblaster, and G. P. Compo, 2003: The Asian monsoon, the tropospheric biennial oscillation, and the Indian Ocean zonal mode in the NCAR CSM. *J. Climate*, **16**, 1617–1642, [https://doi.org/10.1175/1520-0442\(2003\)016<1617:TAMTTB>2.0.CO;2](https://doi.org/10.1175/1520-0442(2003)016<1617:TAMTTB>2.0.CO;2).
- Luo, J.-J., S. Masson, S. Behera, and T. Yamagata, 2007: Experimental forecasts of the Indian Ocean dipole using a coupled OAGCM. *J. Climate*, **20**(10), 2178–2190, <https://doi.org/10.1175/JCLI4132.1>.
- Masumoto, Y., H. Hase, Y. Kuroda, H. Matsuura, and K. Takeuchi, 2005: Intraseasonal variability in the upper layer currents observed in the eastern equatorial Indian Ocean. *Geophys. Res. Lett.*, **32**, L02607, <https://doi.org/10.1029/2004GL021896>.
- Mu, M., W. S. Duan, and B. Wang, 2007: Season-dependent dynamics of nonlinear optimal error growth and El Niño–Southern Oscillation predictability in a theoretical model. *J. Geophys. Res.*, **112**(D10), D10113, <https://doi.org/10.1029/2005JD006981>.
- Mu, M., Y. S. Yu, H. Xu, and T. T. Gong, 2014: Similarities between optimal precursors for ENSO events and optimally growing initial errors in El Niño predictions. *Theor. Appl. Climatol.*, **115**, 461–469, <https://doi.org/10.1007/s00704-013-0909-x>.
- Saji, N. H., and T. Yamagata, 2003: Structure of SST and surface wind variability during Indian Ocean dipole mode events: COADS observations. *J. Climate*, **16**(16), 2735–2751, [https://doi.org/10.1175/1520-0442\(2003\)016<2735:SOSASW>2.0.CO;2](https://doi.org/10.1175/1520-0442(2003)016<2735:SOSASW>2.0.CO;2).
- Saji, N. H., B. N. Goswami, P. N. Vinayachandran, and T. Yamagata, 1999: A dipole mode in the tropical Indian Ocean. *Nature*, **401**(6751), 360–363, <https://doi.org/10.1038/43854>.
- Snyder, C. M., 1996: Summary of an informal workshop on adaptive observations and FASTEX. *Bull. Amer. Meteor. Soc.*, **77**, 953–961.
- Stuecker, M. F., A. Timmermann, F.-F. Jin, Y. Chikamoto, W. J. Zhang, A. T. Wittenberg, E. Widiasih, and S. Zhao, 2017: Revisiting ENSO/Indian Ocean Dipole phase relationships. *Geophys. Res. Lett.*, **44**, 2481–2492, <https://doi.org/10.1002/2016GL072308>.
- Taylor, K. E., R. J. Stouffer, G. A. Meehl, 2012: An Overview of CMIP5 and the experiment design. *Bull. Amer. Meteor. Soc.*, **93**, 485–498, <https://doi.org/10.1175/BAMS-D-11-00094.1>.
- Vinayachandran, P. N., S. Iizuka, and T. Yamagata, 2002: Indian Ocean dipole mode events in an ocean general circulation model. *Deep Sea Research Part II: Topical Studies in Oceanography*, **49**, 1573–1596, [https://doi.org/10.1016/S0967-0645\(01\)00157-6](https://doi.org/10.1016/S0967-0645(01)00157-6).
- Webster, P. J., A. M. Moore, J. P. Loschnigg, and R. R. Leben, 1999: Coupled ocean–atmosphere dynamics in the Indian Ocean during 1997–1998. *Nature*, **401**(6751), 356–360, <https://doi.org/10.1038/43848>.
- Weiss, J. P., and J. B. Weiss, 1999: Quantifying persistence in ENSO. *J. Atmos. Sci.*, **56**(16), 2737–2760, [https://doi.org/10.1175/1520-0469\(1999\)056<2737:QPIE>2.0.CO;2](https://doi.org/10.1175/1520-0469(1999)056<2737:QPIE>2.0.CO;2).
- Weller, E., and W. J. Cai, 2013a: Asymmetry in the IOD and ENSO teleconnection in a CMIP5 model ensemble and its relevance to regional rainfall. *J. Climate*, **26**, 5139–5149, <https://doi.org/10.1175/JCLI-D-12-00789.1>.
- Weller, E., and W. J. Cai, 2013b: Realism of the Indian Ocean Dipole in CMIP5 models: The implications for climate projections. *J. Climate*, **26**, 6649–6659, <https://doi.org/10.1175/JCLI-D-12-00807.1>.
- Yang, J. L., Q. Y. Liu, and Z. Y. Liu, 2010: Linking observations of the Asian Monsoon to the Indian Ocean SST: Possible roles of Indian Ocean basin mode and dipole mode. *J. Climate*, **23**, 5889–5902, <https://doi.org/10.1175/2010JCLI2962.1>.
- Yoo, S. H., S. Yang, and C. H. Ho, 2006: Variability of the Indian Ocean sea surface temperature and its impacts on Asian–Australian monsoon climate. *J. Geophys. Res.*, **111**, D03108, <https://doi.org/10.1029/2005JD006001>.
- Zheng, X.-T., S.-P. Xie, Y. Du, L. Liu and Q. Y. Liu, 2013: Indian Ocean Dipole response to global warming in the CMIP5 multimodel ensemble. *J. Climate*, **26**, 6067–6080, <https://doi.org/10.1175/JCLI-D-12-00638.1>.